

<https://doi.org/10.1038/s42005-024-01690-x>

# Nonlinear wave propagation in a bistable optical chain with nonreciprocal coupling



Pedro J. Aguilera-Rojas <sup>1</sup>, Karin Alfaro-Bittner <sup>2</sup>, Marcel G. Clerc <sup>1</sup>, Manuel Díaz-Zúñiga <sup>1</sup> ,  
Amaru Moya <sup>1</sup>, David Pinto-Ramos <sup>1</sup> & René G. Rojas <sup>3</sup>

The propagation of nonlinear waves, such as fires, weather fronts, and disease spread, has drawn attention since the dawn of time. A well-known example of nonlinear wave-fronts—in our daily lives is the domino waves, which propagate equally toward the left or right flank due to their reciprocal coupling. However, there are other situations where front propagation is not fully understood, such as bistable fronts with nonreciprocal coupling. These couplings are characterised by the fact that the energy emitter and receiver are not interchangeable. Here, we study the propagation of nonlinear waves in a bistable optical chain forced by nonreciprocal optical feedback. The spatiotemporal evolution and the front speeds are characterised as a function of the nonreciprocal coupling. We derive an equation to describe the interacting optical elements in a liquid crystal light valve with nonreciprocal optical feedback and compare the experimental results with numerical simulations of the coupled bistable systems.

Fires, the spread of diseases, supercooling of water, weather fronts, crystal growth, shock waves, and population migrations, correspond to nonlinear waves called fronts<sup>1–5</sup>. These waves result from the coexistence of equilibria in extended systems, corresponding to spatial connections between them. In fact, fronts and multistability are characteristic features of dissipative nonlinear systems. The concept of front propagation, which originated in the context of population dynamics<sup>6,7</sup>, has since attracted increasing interest in chemistry, physics, and mathematics. One of the relevant differences between linear waves and fronts is that the shape or profile of the fronts does not depend on the initial conditions. Indeed, these nonlinear waves are attractors, so an initial condition connecting two domains converges to a precise profile after some transient. The front speed depends on equilibria they connect; for example, fronts between stable and unstable equilibria in weakly nonlinear systems are characterised by the stable equilibrium invading the unstable one<sup>1,2</sup>. Examples of this type of front are combustion, the spread of persistent infectious diseases, or the freezing of supercooled water, to mention a few. However, in multistable systems with many equilibria, fronts where an unstable state invades a stable one can be observed<sup>8</sup>. The scenario changes radically when considering fronts between two stable states. If the system is variational, the front speed depends on the energy difference between states<sup>9</sup>. Namely, the most stable state invades the least stable one.

Discrete bistable coupled systems can also exhibit fronts, where the main feature is that the fronts propagate with hopping or oscillatory

dynamics<sup>10–12</sup>. A playful example of fronts in our daily lives is domino waves, which is an extended bistable chain system in which a domino has two equilibria, its vertical and horizontal position<sup>13</sup>. Coupled bistable physical systems where front propagation has been observed are calcium release waves in living cells<sup>14,15</sup>, reaction fronts in chains of coupled chemical reactors<sup>16</sup>, arrays of coupled diode resonators<sup>17</sup>, semiconductor superlattices<sup>18</sup>, chains of paramagnetic colloidal particles<sup>19</sup>, covalent chemical reactions on single-walled carbon nanotubes<sup>20</sup>, and the dynamics of neuron chains<sup>21</sup>, to mention a few. In all the above examples, the elements of the chains are usually coupled with reciprocal media (elastic, chemical, or electrical). Namely, if one exchanges the role of emitter and receiver, the observed propagation is the same. Indeed, elastic media are characterised by applying a force of equal magnitude and opposite direction to each of the coupled elements; such dynamical behaviour is known as Maxwell-Betti reciprocity<sup>22–24</sup>.

Due to asymmetric, nonlinear, and/or time nonreversal properties, nonreciprocal behaviour has been studied in several physical fields. In optics, nonreciprocal responses have been observed in birefringent prisms<sup>25</sup>, optomechanical resonators<sup>26</sup>, and asymmetric cavities<sup>27</sup>. In acoustics, an emitter and a receiver can exhibit nonreciprocal behaviours in a resonant ring cavity biased by a circulating fluid<sup>28</sup>. In electronics, a nonreciprocal behaviour has been reported using an electrically driven nonreciprocity on a silicon chip<sup>29</sup>. Nonreciprocal behaviours for the propagation of electromagnetic waves have been accomplished through the application of

<sup>1</sup>Departamento de Física and Millennium Institute for Research in Optics, FCFM, Universidad de Chile, Casilla 487-3, Santiago, Chile. <sup>2</sup>Universidad Rey Juan Carlos, Calle Tulipán s/n, 28933 Móstoles, Madrid, Spain. <sup>3</sup>Instituto de Física, Pontificia Universidad Católica de Valparaíso, Casilla, 4059 Valparaíso, Chile.

e-mail: [manudiaz@ug.uchile.cl](mailto:manudiaz@ug.uchile.cl)

magnetic fields<sup>30,31</sup>, angular momentum<sup>32</sup>, nonlinear coupling<sup>33</sup>, and moving photonic crystal<sup>34</sup>. In active matter, nonreciprocal couplings are a rule rather than an exception<sup>35,36</sup>. Recently, through the use of mechanical metamaterials<sup>37,38</sup>, nonreciprocal coupling elements have been built up. Most of these studies have examined the effect of nonreciprocity on the propagation of linear waves. In particular, propagation is favoured in one direction. A similar phenomenon has been proposed theoretically in non-reciprocally coupled multistable systems, exhibiting fronts between unstable and stable equilibrium with a controllable velocity under no external bias<sup>39</sup>.

Based on an experiment of a bistable optical chain forced by non-reciprocal optical feedback, we can study the propagation of nonlinear waves. Figure 1a and b depict the bistable optical chain. The bistable optical dimer system with reciprocal and nonreciprocal coupling and inter-cell dynamics is shown in Fig. 1c and d. Experimental and theoretical bistability cycle of each cell in the optical chain is illustrated in Fig. 1b. The non-reciprocal optical coupling controls the difference in front speed in one direction or the other. A spatial light modulator allows us to control the reciprocal coupling between the elements of the chain and the initial conditions. A shift in the optical feedback induces nonreciprocity in the coupling, which we coin nonreciprocal optical feedback—also known as translational optical feedback. The spatiotemporal evolution and the front speeds are characterised. Near the reciprocal limit, the front speed is characterised by increasing (decreasing) linearly with the positive (negative)

displacement of the nonreciprocal optical feedback  $\alpha$ , however, as it increases enough, it exhibits a maximum due to the effect of nonlinear nonreciprocal couplings. Theoretically, a bistable system chain model is derived using a tight binding approach for the liquid crystal light valve with nonreciprocal optical feedback. Analytically, one can derive expressions for the front speed in the limit that the nonreciprocal terms are perturbative, which, as one expects, is linear, with the parameter that measures non-reciprocity (see thesis<sup>40</sup>). Numerical simulations of the coupled bistable systems show a good agreement with experimental observations.

## Results

A system that can optically address its bistability range is the liquid crystal light valve with optical feedback<sup>41</sup>. The liquid crystal light valve (LCLV) with optical feedback is a flexible experimental setup that exhibits a wide range of dynamic behaviours, such as multistability, front propagation, pattern formation, localised states, and complex spatiotemporal dynamics<sup>41</sup>. All the aforementioned studies have been developed in a continuous dynamical context. This LCLV is composed of a nematic liquid crystal layer with planar anchoring, a dielectric mirror, and a photosensitive wall. When the liquid crystal light valve is subjected to a constant voltage  $V_0$  and illuminated by a low intensity ( $\sim 1 \text{ mW/cm}^2$ ) laser, the light is reflected, and its polarisation phase contains information about the molecular orientation of the liquid crystal. By injecting this same light onto the photosensitive wall, the

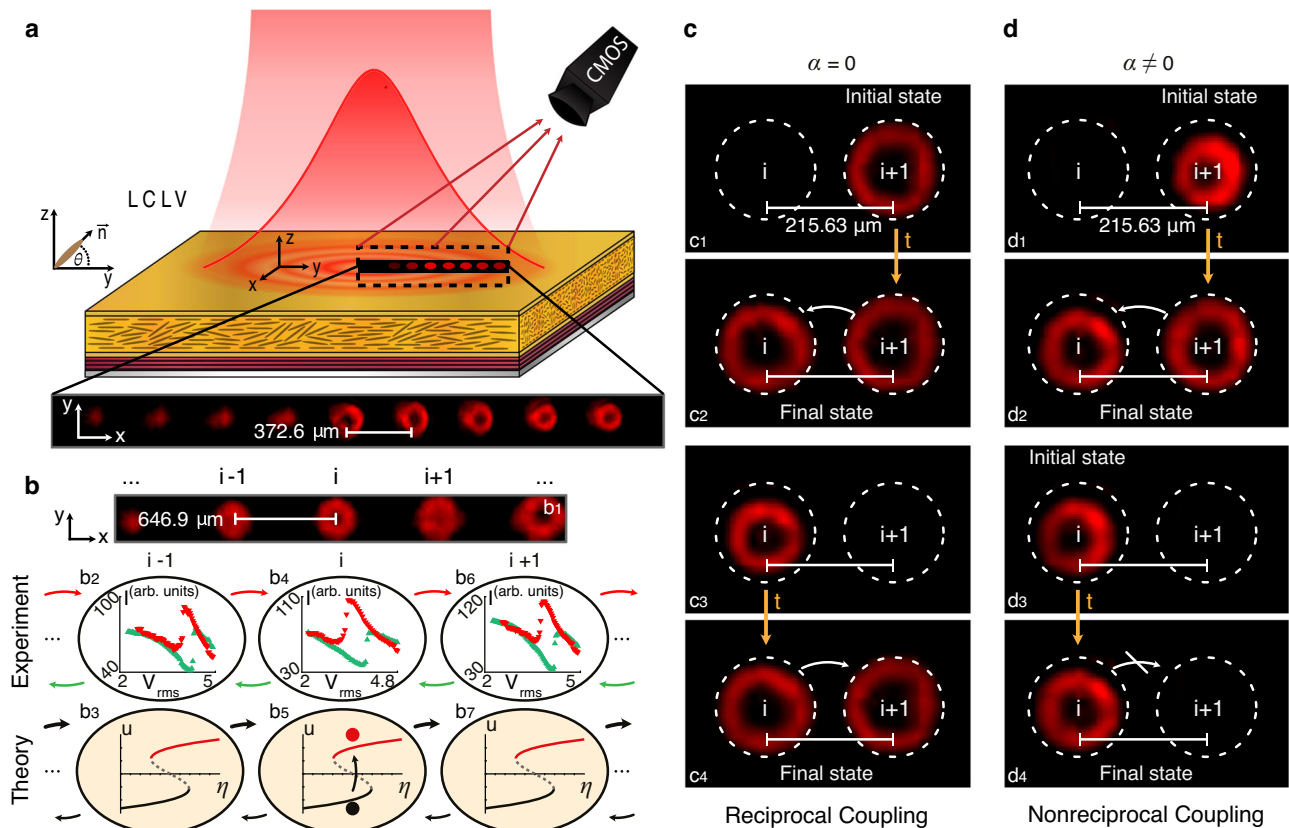


**Fig. 1 | Liquid crystal light valve (LCLV) with reciprocal and nonreciprocal optical feedback.** **a** Schematic representation of a liquid crystal light valve and optical bistable system chain. Scale bar indicates the distance between cells. **b** Snapshot of the optical bistable system chain and schematic representation of dissipative bistable optical chain. Scale bar indicates bistable cell spacing. **b1** Experimental snapshot of the optical bistable system chain. The red spots depict the cells that make up the chain of bistable systems. The colour intensity in these red spots (cells) accounts for different states of molecular orientation, which coexist for the same experimental parameters, a dark and bright one. The index  $i$  labels the different cells. The panels **b2**, **b3**, and **b4** illustrate that each cell undergoes an experimental bistability cycle. The cells are nonreciprocally coupled with their

nearest neighbours. The arrows represent the different magnitudes of the coupling, and red and black dots account for dark and bright cells, respectively. The panels **b5**, **b6**, and **b7** schematise theoretically each bistable cell nonreciprocally coupled to its nearest neighbour. **c**, **d** represent a reciprocally and nonreciprocally coupled bistable system dimer.  $\alpha$  measures the lateral shift of the optical feedback, producing non-reciprocal coupling. The panels **c1**, **c3**, **d1**, and **d3** show the snapshots of the dimer's initial states, and the panels **c2**, **c4**, **d2**, and **d4** show the snapshots of the dimer's final states when one of the cells is excited. The system evolves, exhibiting a clear non-reciprocal coupling. See the Supplementary Movie 1. The dashed circles account for the illuminated areas. The scale bars accurately show the distance between interacting cells.

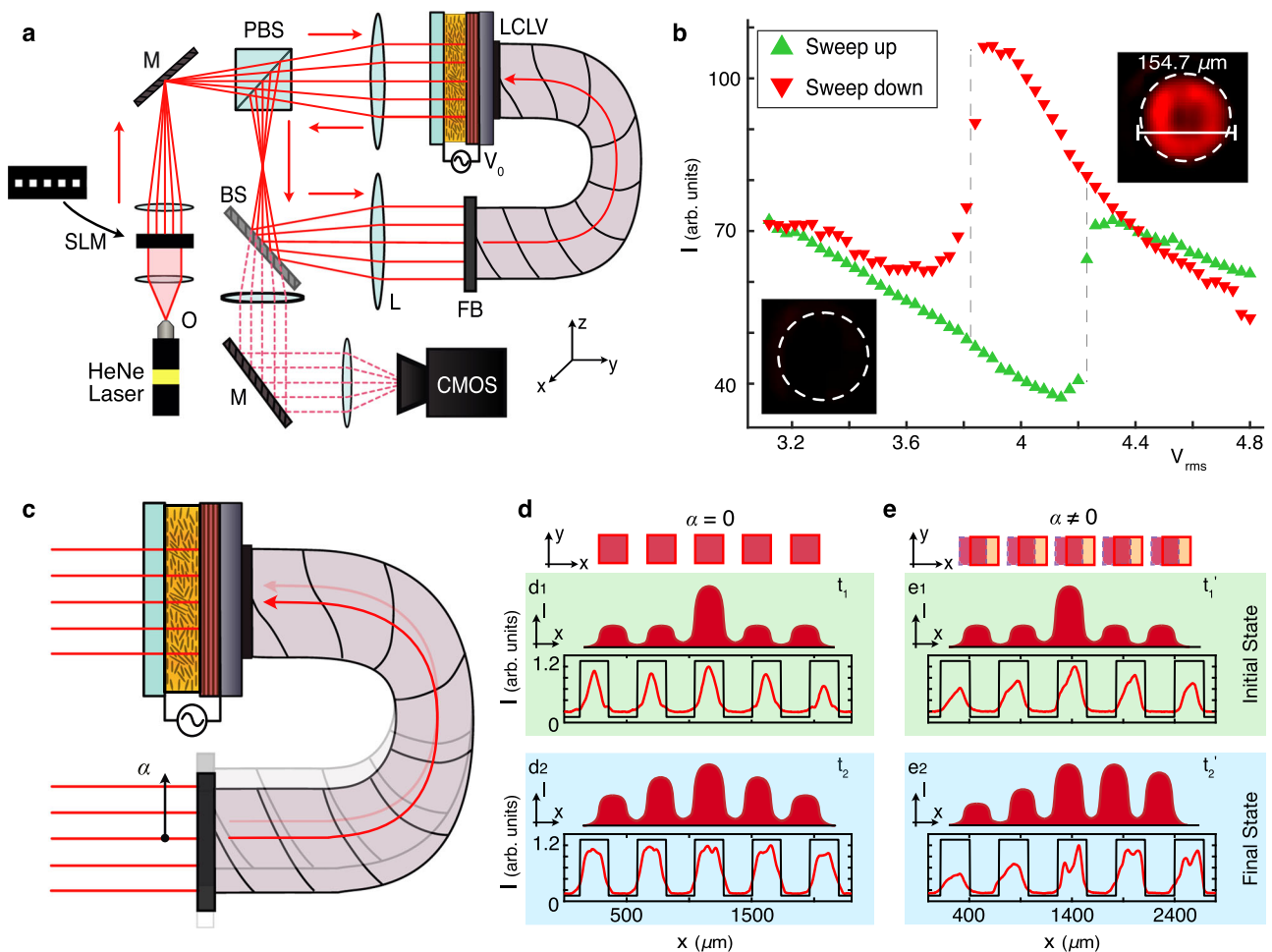


**Fig. 2 | Experimental liquid crystal light valve (LCLV) with reciprocal and nonreciprocal optical feedback.** **a** Experimental scheme of the optical valve. He-Ne Laser accounts for a Helium-Neon laser light source. *O* is an optical objective, SLM is a spatial light modulator, *M* is a mirror, PBS corresponds to a polarizer beam splitter,  $V_0$  is the voltage applied to the LCLV, BS is a beam splitter, *L* stands for lens, FB is a high resolution optical fibre bundle, and CMOS accounts for a Complementary Metal-Oxide-Semiconductor camera. **b** A bifurcation diagram is obtained for a single light cell driven by the laser applied to the optical valve, as the voltage  $V_0$  applied to the valve is varied. The vertical axis represents the total intensity measured in the camera in arbitrary units. The insets are the respective snapshots taken with the camera. The dashed circles account for the illuminated areas. The red and green

triangles show the sweep with the voltage down and up, respectively. The bistability region is highlighted with vertical dashed lines. **c** Schematic illustration of how nonreciprocal optical feedback is generated.  $\alpha$  accounts for the shift of the optical fibre bundle. The scale bar indicates the cell size. The panels **d** and **e** account for the temporal evolution of the intensity profiles from the optical chain system. Panels **d1** and **e1** in the green region account for the initial state profile. Panels **d2** and **e2** in the cyan region account for the final state profile in the intermediate line of the bistable chain with reciprocal and non-reciprocal coupling, respectively. The optical non-reciprocal feedback in the LCLV ( $\alpha \neq 0$ ) is depicted with the displacement between the squares at the top of these panels.

photoconductor at the rear of the optical valve induces an extra voltage on the liquid crystal, which depends on the molecular orientation through the modulated light phase. Figure 2a shows a schematic representation of the experimental setup. As a result of the optical feedback, the optical valve exhibits bistability between two homogeneous states (see Fig. 2b). Each state represents different molecular average orientations, generating the transmission of more or less light due to polarisation interference (cf. to insets in Fig. 2b). Figure 2c shows an experimental schematic illustration of how nonreciprocal coupling is achieved by shifting the optical feedback. Then, when the liquid crystal light valve is illuminated with different light beams that are sufficiently separated, we can induce a chain of reciprocally coupled bistable systems through the evanescent waves of the illuminated spots generated by the molecular reorientation of the liquid crystal. The set of separate light beams is achieved by including a spatial light modulator in the illumination system of the experiment.

By changing the voltage applied to the optical valve, the chain of bistable optical systems is initiated in the lower state of the bistable branch (dark cell). Still, in the parameter range, the most stable state is that of the upper branch (bright cell). By letting more light into one of the beams or by

exploiting imperfections in the liquid crystal (spacers or inhomogeneities), one of the cells is excited to the upper state of the bistability branch, which triggers the propagation of fronts to the sides of the excited cells (see the Supplementary Movie 2). In fact, the neighbouring cells start to light up one after the other, similar to dominoes falling in a domino wave. Figure 2d and e show the initial and final state profile at the midline upon excitation of an intermediate cell in the chain of bistable optical systems.

To determine the speed of the propagation front, we select the cells whose light intensity is greater than a critical value. In the spatiotemporal diagram shown in Fig. 3a, we have marked these critical values with cross symbols and their corresponding error bars. The connection of the points by segmented lines allows us to illustrate front propagation. Note that there is a slight asymmetry in the propagation of the fronts because the illumination is not perfectly homogeneous, but Gaussian as depicted in Fig. 1a.

#### Liquid crystal light valve with nonreciprocal optical feedback

To achieve aligned optical feedback, we use a bundle of optical fibres placed in a position of zero diffraction thanks to a 4f configuration (see Fig. 2a). As a result of the aligned optical feedback, the coupling between the cells of the

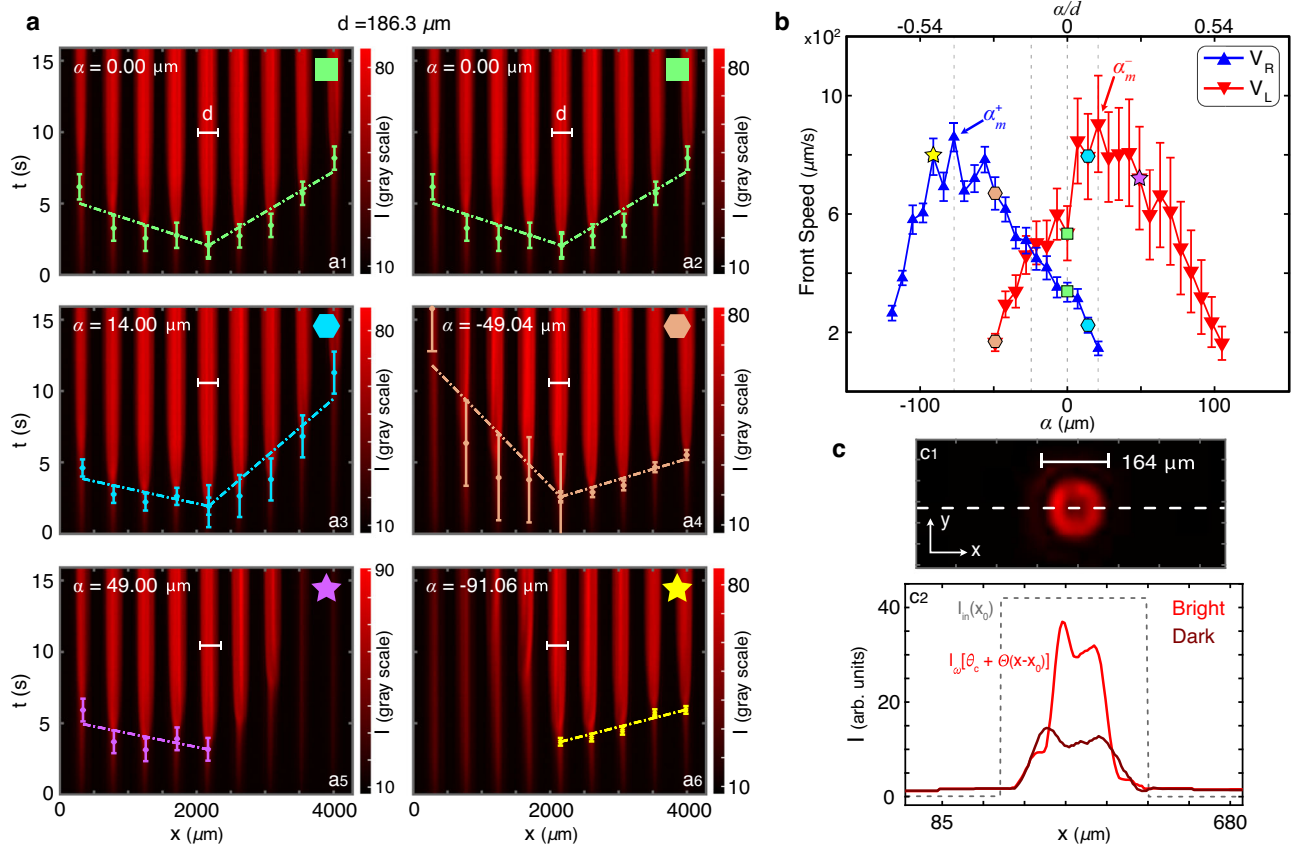


**Fig. 3 | Front propagation in a bistable optical chain with nonreciprocal coupling.** **a** Spatiotemporal diagrams of chains of bistable optical systems with different shifted optical feedback controlled by the displacement  $\alpha$ . The cross with error bars show the moment in which the cells of the bistable system light up. The linear regression and the standard deviation of the crosses are represented by the segmented lines and the error bars, respectively. Most precisely, the error bars represent the least squares error of the linear fit  $t = (x - x_c)/v + t_0$ , where  $x_c$  is the position of the central cell and  $t_0$  is the time at which the central cell is light up. The segmented lines show a linear fit

for the propagation of fronts in the spatiotemporal diagram. The scale bars indicate the cell size. **b** Front speed versus the shift of the optical feedback  $\alpha$ . The blue and red curves show the speed of the front towards the right ( $V_R$ ) and left ( $V_L$ ) flank, respectively.  $\alpha = \alpha_m^\pm$  accounts for the critical value for which it is measured the maximum speed. The symbols squares, hexagons, and stars account for the spatiotemporal diagrams shown in panel **a**. **c** Snapshot of a single bistable cell and corresponding mid-line profile in the dark (ground) and bright (excited) state. The scale bar shows the cell size.

bistable optical chain is reciprocal. To create a nonreciprocal coupling, we proceed by horizontally shifting the fibre bundle to a distance  $\alpha$  (cf. Fig. 2c). This shifting is achieved by a servo motor, which has a precision of the order of microns. This shifted optical feedback causes the evanescent tails of each cell to couple asymmetrically to its neighbours, i.e., it is a nonreciprocal coupling. We can verify the above feature experimentally. Let's consider only two cells, a coupled bistable system dimer. When the coupling is reciprocal, the excitation of one of them causes the excitation of the neighbouring cell, as shown in Fig. 1c. If we include a shifted optical feedback when one cell is excited (see Fig. 1d), let us say cell  $i + 1$ , it excites its neighbour  $i$ , but in the opposite, i.e., excited cell  $i$  cannot excite cell  $i + 1$ .

As a result of the shifted optical feedback, the midline intensity profiles become asymmetrical, as illustrated in Fig. 2e. The propagation of the fronts is now asymmetric, depending on the  $\alpha$  value, we can modify the propagation speed. Figure 3a illustrates the spatiotemporal evolution and the corresponding propagation of the fronts for different  $\alpha$  shifts. From this type of plot, we can determine the speed of the fronts. Figure 3b summarises the velocity of the fronts as a function of the  $\alpha$  shift. As mentioned before, due to the spatially inhomogeneous illumination at  $\alpha = 0$ , the velocities towards the left and right flank do not coincide. We notice that for small nonreciprocal optical feedback, the velocity of the fronts is linearly modified. This can be understood as the nonreciprocal coupling producing a drift-like effect on the fronts. However, for large nonreciprocal couplings, the speed of the fronts exhibits a maximum at  $\alpha = \alpha_m^\pm$ . We associate this phenomenon with nonlinear nonreciprocal couplings. It is important to contrast the

modification of the front speed employing nonreciprocal coupling with the one achieved by an external bias, i.e., by changing the relative stability of equilibria<sup>42</sup>. With nonreciprocal coupling, the left- and right-flank fronts propagate with a different speed, with the difference controlled by the nonreciprocity intensity; however, with an external bias, the left- and right-flank fronts propagate with the same speed, which is controllable by the energy difference between equilibria.

### Theoretical description

The dynamics of the average molecular orientation tilt  $\theta(x, t)$  is described by a nonlocal relaxation equation of the form<sup>41,43</sup>

$$\tau \partial_t \theta = l^2 \partial_{xx} \theta - \theta + \frac{\pi}{2} \left( 1 - \sqrt{\frac{\Gamma V_{FT}}{\Gamma V_0 + \chi I_w(\theta, \alpha)}} \right), \quad (1)$$

where  $x$  and  $t$  are the nonreciprocity direction of the liquid crystal layer and time, respectively.  $\theta(x, t) = 0$  and  $\theta(x, t) = \pi/2$  account for the planar and homeotropic configuration.  $V_{FT} \approx 4.5 V_{rms}$  is the threshold for the Fréedericksz transition at 25°C,  $\tau = 100$  ms is the liquid-crystal relaxation time, and  $l = 30$   $\mu\text{m}$  is the electric coherence length. The light intensity  $I_w$  reaching the photoconductor, namely, the nonreciprocal optical feedback, is given by  $I_w[\theta(x + \alpha)] = I_m(x + \alpha)(1 - \cos[\beta \cos^2(\theta(x + \alpha))])/2$ <sup>41</sup>, where  $I_m(x)$  is the light intensity controlled by the spatial light modulator and  $\beta \approx 2kd\Delta n$ , with  $d = 15$   $\mu\text{m}$  as the thickness of the nematic layer,  $\Delta n = 0.2$  as the liquid crystal



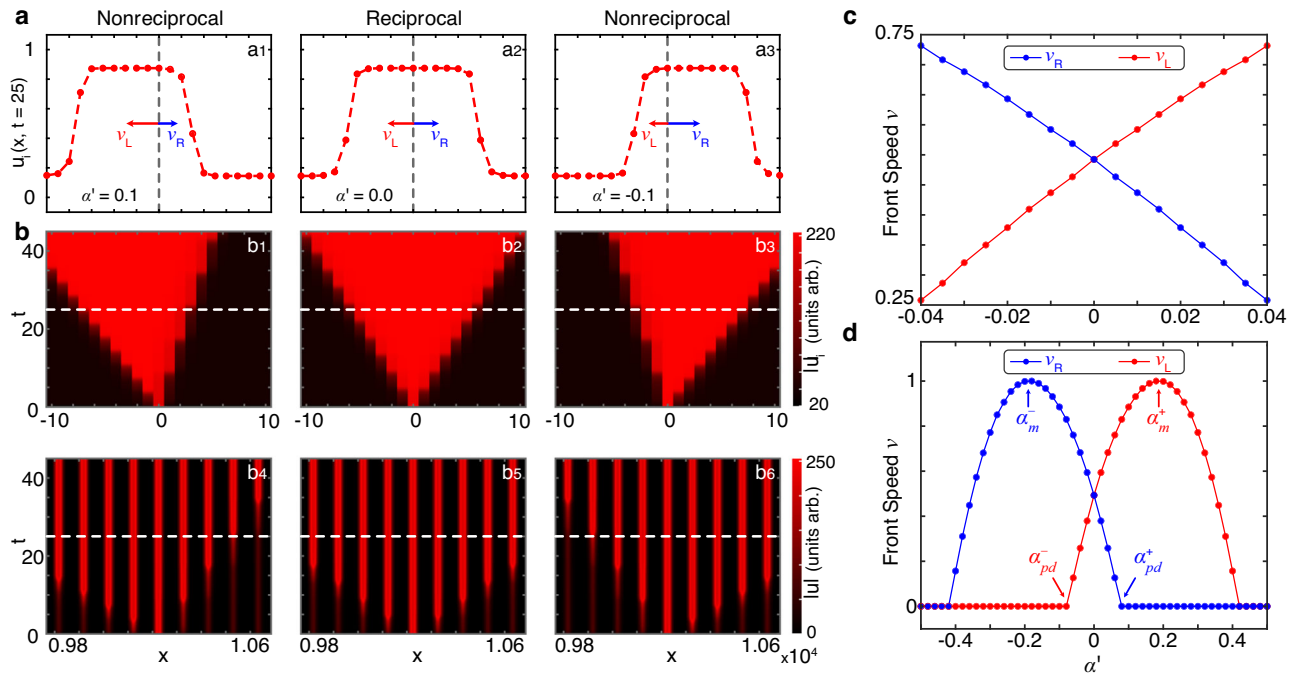


**Fig. 4 | Numerical front propagation in a bistable optical chain with non-reciprocal coupling model Eq. (3) with  $\eta = 0.5$ ,  $\mu = 2.2$ ,  $D = 0.6$ ,  $\kappa_+ = 0.1 + 3\alpha'$ ,  $\kappa_- = 0.1 - 3\alpha'$ , and  $\alpha'$  is the bifurcation parameter. **a** Front profile for different nonreciprocal couplings. Panels **a1**, **a2**, and **a3** show front propagation towards the left, symmetrical, and right flank, respectively. **b** Spatiotemporal diagram of the respective fronts. Panels **b1–b6** account for direct simulations and the nonreciprocal bistable system chain reconstruction. Fronts speed towards the left and right flank as**

a function of the nonreciprocal parameter  $\alpha'$ . Panels **c**, **d** account for small and large nonreciprocal coupling, respectively. The blue and red curves show the front speed towards the right ( $V_R$ ) and left ( $V_L$ ) flank, respectively. The system exhibits a pinning-depinning transition of front nonlinear waves for  $\alpha' = \alpha_{pd}^\pm$ .  $\alpha_m^\pm$  accounts for the critical value for the nonreciprocal coupling parameter with the greatest magnitude observed for the front speed.

birefringence, and  $k = 2\pi/\lambda$  is the wavenumber of the light; we employ a red laser of wavelength  $\lambda = 632.8\text{nm}$ . The effective voltage,  $V_{\text{eff}}$  applied to the liquid crystal layer can be expressed as  $V_{\text{eff}} = \Gamma V_0 + \chi I_w$ ,  $\Gamma = 0.15$  is a transfer factor that depends on the electrical impedances of the photoconductor, dielectric mirror, and liquid crystal while  $\chi$  is a phenomenological dimensional parameter that describes the linear response of the photoconductor<sup>41</sup>.

When the intensity of the illumination light  $I_m$  is varied, model (1) shows different branches of bistability resulting from critical values of the average molecular orientation angle  $\theta_c$ . The spatial light modulator can be used to induce potential wells, or inhomogeneous illumination, that alternates between the bistable and monostable region (planar state), as shown in Fig. 3c represented with the  $I_m(x)$  function, where the maxima and minima of these potential wells correspond to illuminated and unilluminated regions, respectively. The separation and amplitude of the well potentials can be controlled with the spatial light modulator. Looking at a single well, it has two states, representing whether the cell is bright or dark, as shown in Figs. 1b, 2b, and 3c. Figure 3c shows the potential well and the light profiles representing the two different states proportional to  $\Theta(x - x_0)$ , where  $x_0$  accounts for the middle position of the well. In the case of considering modulation wells in the bifurcation parameter that are separated enough, one can use the following ansatz to describe the dynamics of each cell (tight binding-like approach),

$$\theta(x, t) = \theta_c + \sum_i u_i(t)\Theta(x - x_i) + W(x_i, u_i, x), \quad (2)$$

where  $u_i(t)$  is the intensity of the average molecular orientation tilt profile in the  $i$ -cell,  $x_i$  is the middle position of the  $i$ -cell, and  $W(x_i, u_i, x)$  is the small correction function that accounts for the effects of the other cells in the  $i$ -cell. Introducing the previous ansatz into Eq. (1), linearizing in  $W$ , and imposing a solvability condition after straightforward calculations, we obtain at

dominant order the following chain of nonlinear, nonreciprocally coupled bistable systems

$$\partial_t u_i = \eta + \mu u_i - u_i^3 + (D + \alpha')(u_{i+1} - u_i) + (D - \alpha')(u_{i-1} - u_i) - (\kappa_+ u_{i+1} + \kappa_- u_{i-1})u_i^2. \quad (3)$$

The Methods section explicitly gives complete and detailed expressions of these coefficients as a function of the liquid crystal light valve parameters.  $u_i$  positive (negative) accounts for the bright (dark) state of the  $i$ -cell (cf. Fig. 1b).  $\eta$  is the bifurcation parameter that characterises and runs through the hysteresis loop, and both states are equivalent when  $\eta = 0$ , Maxwell's point.  $\mu$  controls the width of the hysteresis.  $D$  and  $\alpha'$  account for reciprocal and nonreciprocal coupling, respectively. The liquid crystal elastic coupling and the nonreciprocal optical feedback effect determine  $D$  and  $\alpha'$ , respectively. Indeed,  $\alpha'$  is proportional to  $\alpha$ .  $\kappa_+$  and  $\kappa_-$  account for the nonlinear nonreciprocal coupling to the right and left flank, respectively, and are proportional to  $\alpha'$ .

Numerical simulations of the chain of bistable systems in the bistability regime show front propagation, where the most stable state invades the least stable one (see Fig. 4). Figure 4a shows different fronts observed with negative, zero, and positive nonreciprocal coupling  $\alpha'$ . The spatiotemporal diagrams associated with the propagation of these fronts is shown in Fig. 4b. Likewise, we have characterised the front speed towards both the left and right flanks as a function of nonreciprocal coupling (cf. Fig. 4c). From this chart, we conclude that when the nonreciprocal coupling is zero, the propagation towards both flanks is symmetric. By including a small nonreciprocal coupling, we observe that the speed of the fronts is linearly modified, favouring one of the flanks. As the nonreciprocal coupling increases, the front speed in the less favoured direction decreases. Numerically, we observe a critical value  $\alpha' = \alpha_{pd}^\pm$  in which the front cannot propagate towards that flank; that is, the system exhibits a phenomenon of pinning-depinning transition<sup>42,44,45</sup>. Hence, for larger nonreciprocal

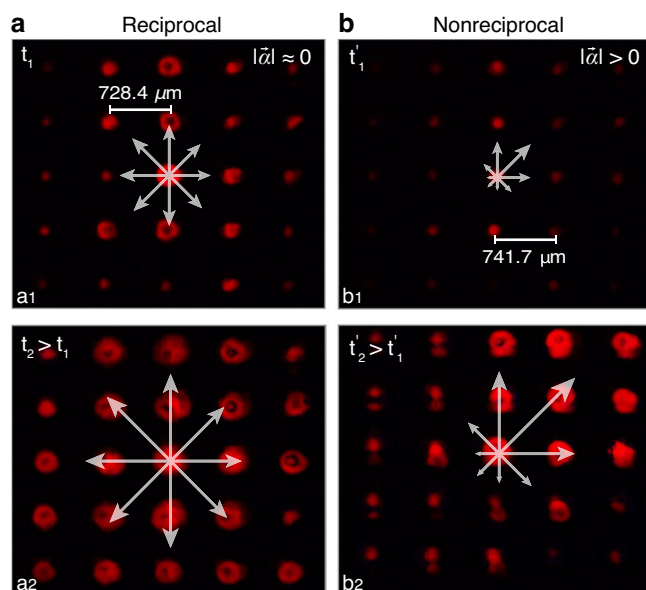


**Fig. 5 | Experimental front propagation in two-dimensional bistable lattice systems.** **a** Square lattice of bistable optical cells with reciprocal coupling. **b** Square lattice of bistable optical cells with non-reciprocal coupling. **a1** and **b1** show the initial conditions  $t_1 = t'_1 = 0$  s. **a2** and **b2** show the final states  $t_2 = 2.52$  s and  $t'_2 = 5.08$  s. The arrows account for the propagation speed in the respective direction. The distance between cells is indicated by the scale bar.

couplings, only one-way propagation is observed. A similar phenomenon is reported for the propagation of linear waves<sup>46</sup>. On the other hand, the front speed in the favoured direction increases up to a critical value  $\alpha' = \alpha_m^\pm$ , after which the front speed decreases. This phenomenon is observed as a consequence of the nonlinear, nonreciprocal coupling terms. Note that the same phenomenon is observed experimentally (see Fig. 3b).

### Two-dimensional nonlinear wave propagation in a bistable optical chain

We can also create a two-dimensional bistable systems lattice thanks to the spatial light modulator. Figure 5 shows the square lattice and the nonlinear wave propagation for reciprocal and nonreciprocal coupling. The arrows account for the propagation speed in the respective direction. In the case of reciprocal coupling, we experimentally observe that the fronts propagate isotropically in all directions (see Fig. 5a). In contrast, in the nonreciprocal case, the nonlinear waves propagate in the direction that the nonreciprocal coupling privileges, which can be easily controlled by a two-dimensional shift of the optical feedback (see Fig. 5b). The Supplementary Movie 3 depicts front propagation in a two-dimensional bistable lattice with and without nonreciprocal coupling.

### Discussion

The waves that connect different equilibria have entirely different characteristics compared to linear waves, because after a transient, these waves converge to a precise spatial shape, and their speed depends on the states they connect and the coupling or transport mechanism. Fronts are relevant in various fields of knowledge, such as chemistry, biology, physics, and optics. Most studies have investigated fronts in continuous media, but fronts are also observed in extended coupled systems. One of the difficulties of coupling discrete systems by means of elastic, magnetic, or optical elements is that the couplings are usually reciprocal. Therefore, the fronts propagate isotropically. Different strategies have been proposed to generate nonreciprocal couplings. We propose that optical feedback in a chain using a photosensitive system achieves manipulable nonreciprocal couplings that can even be coupled to more distant neighbours. Therefore, this type of coupling opens the possibility of studying nonreciprocal

effects in one- and two-dimensional systems. Most studies of nonreciprocal effects have been carried out on linear waves; here, we have studied the impact of nonreciprocal coupling on fronts, a type of nonlinear wave. As a result of nonreciprocal coupling, the fronts propagate in privileged directions; the propagation of waves in certain directions can even be prevented. This opens up the possibility of isolating regions and directing energy propagation, which, in this case, is carried by light intensity. A systematic study of the pinning-depinning transition of fronts due to nonreciprocal coupling and its potential implications for energy manipulation are in progress.

At the same time, nonlinear nonreciprocal effects have hardly been studied. We observe that these terms are responsible for increasing, decreasing, and even cancelling the propagation of fronts. Theoretically, nonreciprocal terms are expected to induce instabilities in fronts, which may even induce the formation of travelling patterns and complex spatio-temporal behaviours.

One of the difficulties of optical couplings is that the light is transversally inhomogeneous due to the Gaussian profile of laser beams; additionally, the free propagation of light generates transversal gradients, which can induce inhomogeneities in the couplings. Hence, front speed in these optical systems could be better described by trajectories other than straight lines, such as parabolic ones, that are being studied.

For simplicity, we have considered the nonlinear wave propagation in a square lattice, but the spatial light modulator is a flexible optical element that allows us to create different regular, disordered, or even quasi-crystalline spatial lattices. Likewise, translating and rotating the optical fibre bundle can achieve more complicated couplings between the lattice elements. Studies of the nonreciprocal effects of this type of lattice may be of interest in understanding complex systems such as complex networks employing a controllable experimental setup.

### Methods

#### Experimental setup

The liquid crystal light valve consists of a nematic liquid crystal LC-654 (NIOPIK) with dielectric anisotropy constant  $\epsilon_a = 10.7 \epsilon_0$  ( $\epsilon_0$  dielectric constant of the vacuum) placed between two glass layers separated by a distance  $d = 15 \mu\text{m}$ . Transparent indium tin oxide (ITO) electrodes and a photoconductive layer are deposited on the glasses to subject the liquid crystal to a driven voltage. A dielectric Bragg mirror with optimised reflectivity for 632.8 nm light is placed in the back layer of the liquid crystal cell. The liquid crystal has planar anchoring in the diagonal direction of the cell; that is, the molecules on the cell wall are attached parallel to the wall. The LCLV can be electrically driven by applying an oscillatory voltage  $V_0$  rms and frequency  $f_0 = 1.0$  kHz across the liquid crystal layer. Figure 2a shows a schematic representation of the LCLV with an optical feedback setup. The valve is optically forced with a He-Ne laser,  $\lambda_0 = 632.8$  nm. The LCLV is placed in a  $4f$  optical configuration ( $f = 25$  cm), as indicated in Fig. 2. The optical feedback circuit is closed with an optical fibre bundle (FB) placed at a distance of  $4f$  from the LCLV front face. The optical fibre bundle injects the light into the photoconductive layer, applying an additional voltage to the liquid crystal material depending on the local light intensity. The optical feedback loop is designed so that light simultaneously presents polarisation interference induced by the polarising beam splitter (PBS) and shift of light over a distance  $\alpha$ . This distance is controlled by a servo motor (Thorlabs Z825B - 25 mm Motorized Actuator with Ø3/8" Barrel). A spatial light modulator (SLM, LC 2012 Spatial Light Modulator Holoeye, transmission) is considered to carry out different configurations of bistable optical chains. This SLM is based on a twisted nematic liquid crystal display, which generates a simple phase modulation and a coupled polarisation effect, resulting likewise in amplitude modulation. The experiment is monitored by a complementary metal-oxide-semiconductor (CMOS) camera. The path and optical elements used for the light beam monitored by the camera are such that we observe the surface of the liquid crystal light valve so that the intensity  $I_w$  can be related to the average angle  $\theta(x, t)$  by  $I_w[\theta] = I_m(x)(1 - \cos[\beta \cos^2 \theta])/2$ .

To generate the bistable system chain with different configurations, the liquid crystal light valve with optical feedback must be illuminated in different space regions. This is achieved through spatial light modulation in transmission, which is illuminated with an expanded beam, allowing only a discrete number of thin beams separated at equal distances to pass. The different beam distributions are achieved by using different masks generated on the SLM through adequate software that controls it.

To generate the initial conditions that produce the propagation of the nonlinear waves, we have used the following procedure: (i) Randomly distributed glass bead spacers are used to maintain the constant thickness inside the liquid crystal cell. (ii) Using the SLM, we have considered a region of space where one of the bistable cells inside contains a glass bead. (iii) Increasing the voltage from the cell with a glass bead induces a bright state, which begins to invade the system. This procedure guarantees that the front emerges regularly from the same cell, which allows us a systematic study of the propagation of nonlinear waves to be carried out.

### Derivation of bistable chain model

The model Eq. (1) is characterised by exhibiting several branches of bistability<sup>41</sup>. To have a simple description of the dynamics of a liquid crystal light valve with nonreciprocal feedback, we consider the dynamics of the model Eq.(1) around the emergence of bistability, i.e., when the average molecular angle equilibrium  $\theta_c(V_0, I_{in})$  becomes multi-valued while illuminated homogeneously (see ref. 43). This angle, as a function of parameters, satisfies the relation

$$V_0 = \frac{V_{FT}}{(1 - \frac{2\theta_0}{\pi})^2} - \frac{\chi I_{in}}{2\Gamma} [1 - \cos(\beta \cos^2 \theta_0)], \quad (4)$$

from this relation, we determine the values of the parameters for the emergence of bistability. In fact, in the parameter space, the above expression generates a folded surface from which one can geometrically deduce the points of emergence of bistability. Namely,  $\theta_0$  becomes multi-valued when the function  $V_0(\theta_0, I_{in})$  has a saddle point. Moreover, around the saddle point  $V_0(\theta_c)$  creates two new extreme points that determine the width of the bistability region.

To find the saddle points of the  $V_0(\theta_c)$  function, we impose the conditions  $dV_0/d\theta_c = 0$ ,  $d^2V_0/d\theta_c^2 = 0$  and, after straightforward calculations, we obtain the relations

$$I_{in}^c = \frac{-\pi^2 \Gamma V_{FT}}{\chi \beta (\pi/2 - \theta_c)^3 \sin(2\theta_c) \sin(\beta \cos^2 \theta_c)}, \quad (5)$$

and

$$\frac{3}{(\frac{\pi}{2} - \theta_c)} - 2 \cot 2\theta_c = -\beta \sin(2\theta_c) \cot(\beta \cos^2 \theta_c). \quad (6)$$

The first expression, Eq. (5), gives the critical value of  $I_{in}$  for which  $\theta_c$  becomes multi-valued. The second expression, Eq. (6), is an algebraic equation that depends only on the parameter  $\beta$  and determines all the points of nascent bistability. The interception points of the two curves correspond to all the points of nascent bistability that can be found for this value of  $\beta$ . However, only half of them have physical significance because the other half correspond to negative intensity values. The dynamics near a nascent bistability point is described by a scalar field governed by a cubic non-linearity. Hence, close to a given point of nascent bistability,  $I_{in} \equiv I_{in}^c$ , and  $V_0 \equiv V_0^c$ , we can approximate the average director tilt field by the expression

$$\theta(x, t) \approx \theta_c + \frac{\phi(x, t)}{\phi_0}, \quad (7)$$

where  $\phi(x, t)$  is an order parameter that accounts for the dynamics around the point of nascent bistability and  $\phi_0^2 \equiv 12/(\pi/2 - \theta_c)^2 + 4 +$

$6 \cos 2\theta_c \cot(\beta \cos^2 \theta_c) - \beta^2 \sin^2 2\theta_c$  is a normalisation constant introduced to simplify the equation for the field  $\phi$ . Introducing the above expression into Eq. (1), considering the 1D case and developing in the Taylor series by keeping the cubic terms, after straightforward algebraic calculations, we can reduce the full liquid crystal light valve with an optical feedback model to a forced dissipative  $\phi^4$ -model, which reads as

$$\tau \partial_t \phi = \eta' + \varepsilon \phi - \phi^3 + l^2 \partial_{xx} \phi, \quad (8)$$

where

$$\frac{\eta'}{\phi_0} \equiv \frac{2}{\pi^2 \Gamma V_{FT}} \left( \frac{\pi}{2} - \theta_c \right)^3 [\Gamma(V_0 - V_0^c) + \chi(1 - \cos(\beta \cos^2 \theta_c))(I_{in} - I_{in}^c)]$$

$$\varepsilon \equiv -(\pi/2 - \theta_c) \left\{ \frac{6(V_0 - V_0^c)}{\pi^2 V_{FT}} + [\beta(\pi/2 - \theta_0) (\sin(2\theta_c) \sin(\beta \cos^2 \theta_c)) + 3(1 - \cos(\beta \cos^2 \theta_c))] \frac{\chi(I_{in} - I_{in}^c)}{\pi^2 \Gamma V_{FT}} \right\}.$$

Thanks to the spatial light modulator through periodically separated beam lighting, we can induce that the parameters are modulated periodically  $\varepsilon(x)$  and  $\eta(x)$ , generating well-type potentials. Considering a single-well potential (the system is illuminated with a single beam) in the parameters and the bistability region, the system exhibits a fundamental mode-type solution  $\Theta(x - x_0)$  where  $x_0$  is the central part of the single-well potential, see Fig. 3c.

Introducing the ansatz (2) and  $\phi(x, t) \rightarrow \phi(x - \alpha, t)$  into Eq. (8), linearizing in  $W$ , and imposing a solvability condition after straightforward calculations, we obtain at dominant order the bistable systems chain

$$\partial_t u_i = \eta + \mu u_i + \Gamma_+ (u_{i+1} - u_i) + \Gamma_- (u_{i-1} - u_i) - (\kappa_+ u_{i+1} + \kappa_- u_{i-1}) u_i^2 - a u_i^3, \quad (9)$$

where

$$\begin{aligned} \eta &= \frac{\langle \eta'(x) | \Theta(x - x_i) \rangle}{\langle \Theta(x - x_i) | \Theta(x - x_i) \rangle}, \\ D + \alpha' &= \Gamma_+ \equiv \frac{\langle \varepsilon(x) \Theta(x - x_{i+1} - \alpha) + l^2 \partial_{xx} \Theta(x - x_{i+1} - \alpha) | \Theta(x - x_i) \rangle}{\langle \Theta(x - x_i) | \Theta(x - x_i) \rangle}, \\ D - \alpha' &= \Gamma_- \equiv \frac{\langle \varepsilon(x) \Theta(x - x_{i-1} - \alpha) + l^2 \partial_{xx} \Theta(x - x_{i-1} - \alpha) | \Theta(x - x_i) \rangle}{\langle \Theta(x - x_i) | \Theta(x - x_i) \rangle}, \\ \mu &= \frac{\langle \varepsilon(x) \Theta(x - x_i - \alpha) + l^2 \partial_{xx} \Theta(x - x_i - \alpha) | \Theta(x - x_i) \rangle}{\langle \Theta(x - x_i) | \Theta(x - x_i) \rangle} + \Gamma_+ + \Gamma_-, \\ \kappa_{\pm} &= 3 \frac{\langle \Theta^2(x - x_i - \alpha) \Theta(x - x_{i\pm 1} - \alpha) | \Theta(x - x_i) \rangle}{\langle \Theta(x - x_i) | \Theta(x - x_i) \rangle}, \\ a &= \frac{\langle \Theta(x - x_i - \alpha)^3 | \Theta(x - x_i) \rangle}{\langle \Theta(x - x_i) | \Theta(x - x_i) \rangle}, \end{aligned} \quad (10)$$

the symbol  $\langle f | g \rangle \equiv \int f(x)g(x)dx$ . Note that  $D = (\Gamma_+ + \Gamma_-)/2$ ,  $\alpha' = (\Gamma_+ - \Gamma_-)/2$ , and for small  $\alpha$ ,  $\kappa_{\pm}$  is proportional to  $\alpha$ . Normalising  $u_i \rightarrow u_i/\sqrt{a}$ ,  $\eta \rightarrow \eta\sqrt{a}$ , and  $\kappa_{\pm} \rightarrow \kappa_{\pm}/\sqrt{a}$ , we obtain Eq. (3).

### Numerical simulations

All the numerical simulations of Eq. (3) were conducted using a fourth-order Runge-Kutta method for the time evolution with Neumann boundary conditions.

To reconstruct the dynamics observed in the chain of nonreciprocal bistable systems, we have partitioned the linear space between active (illuminated) and non-active (non-illuminated) cells. In each active cell, we have

graphed the evolution of the  $i$ -cell as follows,

$$u(x, t) = u_i(t) \sqrt{\varepsilon_0} \operatorname{sech}^2 \left( \frac{x - x_i}{\sqrt{\varepsilon_0}} \right), \quad (11)$$

where  $\varepsilon_0$  is the typical width of the cell.

## Data availability

The data that support the findings of this study are available from the corresponding author upon reasonable request.

## Code availability

The code used for the analysis is available from the corresponding author upon reasonable request.

Received: 9 January 2024; Accepted: 5 June 2024;

Published online: 17 June 2024

## References

- Murray, J. D. *Mathematical Biology: II: Spatial Models and Biomedical Applications*. (Springer: New York, 2003).
- Saarloos, W. V. Front propagation into unstable states. *Phys. Rep.* **386**, 29 (2003).
- Collet, P. & Eckmann, J. P. *Instabilities and Fronts in Extended Systems*. (Princeton University Press, Princeton, 1990).
- Pismen, L. M. *Patterns and Interfaces in Dissipative Dynamics*. (Springer: Berlin, 2006).
- Mendez, V., Fedotov, S. & Horsthemke, W. *Reaction-transport systems: mesoscopic foundations, fronts, and spatial instabilities*. (Springer Science & Business Media, Berlin, 2010).
- Fisher, R. A. The wave of advance of advantageous genes. *Ann. Eugen.* **7**, 355 (1937).
- Kolmogorov, A., Petrovsky, I. & Piskunov, N. Investigation of the equation of diffusion combined with increasing of the substance and its application to a biology problem. *Bull. Univ. Moscow Ser. Int. Sec. A* **1**, 1 (1937).
- Castillo-Pinto, C., Clerc, M. G. & González-Cortés, G. Extended stable equilibrium invaded by an unstable state. *Sci. Rep.* **9**, 15096 (2019).
- Pomeau, Y. Front motion, metastability and subcritical bifurcations in hydrodynamics. *Phys. D.* **23**, 3 (1986).
- Ishimori, Y. & Munakata, T. Kink dynamics in the discrete Sine-Gordon system a perturbational approach. *J. Phys. Soc. Jpn.* **51**, 3367 (1982).
- Peyrard, M. & Kruskal, M. D. Kink dynamics in the highly discrete sine-Gordon system. *Phys. D.* **14**, 88 (1984).
- Clerc, M. G., Elías, R. G. & Rojas, R. G. Continuous description of lattice discreteness effects in front propagation. *Philos. Trans. R. Soc. A* **369**, 412 (2011).
- Eftimiou, C. J. & Johnson, M. D. Domino waves. *SIAM Rev.* **49**, 111 (2007).
- Dawson, S. P., Keizer, J. & Pearson, J. E. Fire-diffuse-fire model of dynamics of intracellular calcium waves. *Proc. Natl Acad. Sci. USA* **96**, 6060 (1999).
- Bugrim, A. E., Zhabotinsky, A. M. & Epstein, I. R. Calcium waves in a model with a random spatially discrete distribution of  $\text{Ca}^{2+}$  release sites. *Biophys. J.* **73**, 2897 (1997).
- Laplanche, J. P. & Erneux, T. Propagation failure in arrays of coupled bistable chemical reactors. *J. Phys. Chem.* **96**, 4931 (1992).
- Löcher, M., Cigna, D. & Hunt, E. R. Noise sustained propagation of a signal in coupled bistable electronic elements. *Phys. Rev. Lett.* **80**, 5212 (1998).
- Amann, A. & Schöll, E. Bifurcations in a system of interacting fronts. *J. Stat. Phys.* **119**, 1069 (2005).
- Martinez-Pedrero, F., Tierno, P., Johansen, T. H. & Straube, A. V. Regulating wave front dynamics from the strongly discrete to the continuum limit in magnetically driven colloidal systems. *Sci. Rep.* **6**, 19932 (2016).
- Deng, S. et al. Confined propagation of covalent chemical reactions on single-walled carbon nanotubes. *Nat. Comm.* **2**, 382 (2011).
- McLaughlin, D., Shapley, R., Shelley, M. & Wieldaard, D. J. A neuronal network model of macaque primary visual cortex (V1): orientation selectivity and dynamics in the input layer 4Ca. *Proc. Natl Acad. Sci. USA* **97**, 8087 (2000).
- Maxwell, J. C. On the calculation of the equilibrium and stiffness of frames. *Philos. Mag. Ser. 5*, 294 (1864).
- Betti, E. Teoria della elasticità, *Il Nuovo Cimento* 7–8, 158 (1872).
- Nassar, H. et al. Nonreciprocity in acoustic and elastic materials. *Nat. Rev. Mater.* **5**, 667 (2020).
- Alekseeva, L. V., Povkh, I. V., Stroganov, V. I., Kidyarov, B. I. & Pasko, P. G. A nonreciprocal optical element. *J. Opt. Technol.* **70**, 525 (2003).
- Mirza, I. M., Ge, W. & Jing, H. Optical nonreciprocity and slow light in coupled spinning optomechanical resonators. *Opt. Expr.* **27**, 25515 (2019).
- Yang, P. et al. Realization of nonlinear optical nonreciprocity on a few-photon level based on atoms strongly coupled to an asymmetric cavity. *Phys. Rev. Lett.* **123**, 233604 (2019).
- Fleury, R., Sounas, D. L., Sieck, C. F., Haberman, M. R. & Alú, A. Sound isolation and giant linear nonreciprocity in a compact acoustic circulator. *Science* **343**, 516 (2014).
- Lira, H., Yu, Z., Fan, S. & Lipson, M. Electrically driven nonreciprocity induced by interband photonic transition on a silicon chip. *Phys. Rev. Lett.* **109**, 033901 (2012).
- Wang, Z., Chong, Y., Joannopoulos, J. D. & Soljacic, M. Observation of unidirectional backscattering-immune topological electromagnetic states. *Nat. (Lond.)* **461**, 772 (2009).
- Haldane, F. D. M. & Raghu, S. Possible realization of directional optical waveguides in photonic crystals with broken time-reversal symmetry. *Phys. Rev. Lett.* **100**, 013904 (2008).
- Sounas, D. L., Caloz, C. & Alú, A. Giant non-reciprocity at the subwavelength scale using angular momentum-biased metamaterials. *Nat. Commun.* **4**, 2407 (2013).
- Lepri, S. & Casati, G. Asymmetric Wave Propagation in Nonlinear Systems. *Phys. Rev. Lett.* **106**, 164101 (2011).
- Wang, D.-W. et al. Optical Diode Made from a Moving Photonic Crystal. *Phys. Rev. Lett.* **110**, 093901 (2013).
- Nagy, M., Ákos, Z., Biro, D. & Vicsek, T. Hierarchical group dynamics in pigeon flocks. *Nat. (Lond.)* **464**, 890 (2010).
- Ginelli, F. et al. Intermittent collective dynamics emerge from conflicting imperatives in sheep herds. *Proc. Natl Acad. Sci. USA* **112**, 12729 (2015).
- Coulaes, C., Sounas, D. & Alú, A. Static non-reciprocity in mechanical metamaterials. *Nat. (Lond.)* **542**, 461 (2017).
- Jin, L. et al. Guided transition waves in multistable mechanical metamaterials. *Proc. Natl Acad. Sci. USA* **117**, 2319 (2020).
- Pinto-Ramos, D., Alfaro-Bittner, K., Clerc, M. G. & Rojas, R. G. Nonreciprocal coupling induced self-assembled localized structures. *Phys. Rev. Lett.* **126**, 194102 (2021).
- Pinto-Ramos, D., *Self-organization induced by nonreciprocal coupling in nonlinear systems* (Ph.D. thesis dissertation at the University of Chile, <https://repositorio.uchile.cl/handle/2250/197401>)
- Residori, S. Patterns, fronts and structures in a liquid-crystal-light-valve with optical feedback. *Phys. Rep.* **416**, 201 (2005).
- Carpio, A. & Bonilla, L. L. Wave front depinning transition in discrete one-dimensional reaction-diffusion systems. *Phys. Rev. Lett.* **86**, 6034 (2001).
- Alvarez-Socorro, A. J., Clerc, M. G., González-Cortés, G. & Wilson, M. Nonvariational mechanism of front propagation: Theory and experiments. *Phys. Rev. E* **95**, 010202(R) (2017).
- Carpio, A. & Bonilla, L. L. Depinning transitions in discrete reaction-diffusion equations. *SIAM J. Appl. Math.* **63**, 1056 (2003).



45. Clerc, M. G., Elias, R. G. & Rojas, R. G. Continuous description of lattice discreteness effects in front propagation. *Philos. Trans. R. Soc. A* **369**, 1 (2011).
46. Brandenbourger, M., Locsin, X., Lerner, E. & Coulais, C. nonreciprocal robotic metamaterials. *Nat. Commun.* **10**, 4608 (2019).

## Acknowledgements

P.J.A-R, M.G.C., M.D-Z., A.M., and D.P-R. are thankful for the financial support of ANID-Millennium Science Initiative Program-ICN17\_012 (MIRO) and FONDECYT 1210353 project. D.P-R. thanks the financial support of ANID by Beca Doctorado Nacional 21201484

## Author contributions

P.J.A-R: Realisation, construction and improvement of the experimental setup. Experimental measurements. Data analysis. Analytical calculations of the theoretical model. Prepared the figures. Review and editing. K.A-B: Development of the front propagation theory. Prepared the figures. Review and editing. M.G.C: Conceptualisation and conception of the problem. Original idea and development of theoretical model. Funding acquisition. Supervision. Original draft. Writing, review, and editing. M.D-Z: Improvement of the experimental setup. Experimental measurements. Data analysis. Numerical simulations. Prepared the figures. Review and editing. A.M: Preliminary experimental measurements. Review and editing. D.P-R: Development of the front propagation theory. Analytical calculations of the theoretical model. Numerical simulations. Review and editing. R.G.R: Development of the front propagation theory. Analytical calculations of the theoretical model. Review and editing. All experiments, theory, and simulations were carried out in Chile, at Laboratorio de Fenómenos Robustos en Óptica (LAFER).

## Competing interests

The authors declare no competing interests.

## Additional information

**Supplementary information** The online version contains supplementary material available at <https://doi.org/10.1038/s42005-024-01690-x>.

**Correspondence** and requests for materials should be addressed to Manuel Díaz-Zúñiga.

**Peer review information** *Communications Physics* thanks May Mei and the other, anonymous, reviewer(s) for their contribution to the peer review of this work.

**Reprints and permissions information** is available at <http://www.nature.com/reprints>

**Publisher's note** Springer Nature remains neutral with regard to jurisdictional claims in published maps and institutional affiliations.

**Open Access** This article is licensed under a Creative Commons Attribution 4.0 International License, which permits use, sharing, adaptation, distribution and reproduction in any medium or format, as long as you give appropriate credit to the original author(s) and the source, provide a link to the Creative Commons licence, and indicate if changes were made. The images or other third party material in this article are included in the article's Creative Commons licence, unless indicated otherwise in a credit line to the material. If material is not included in the article's Creative Commons licence and your intended use is not permitted by statutory regulation or exceeds the permitted use, you will need to obtain permission directly from the copyright holder. To view a copy of this licence, visit <http://creativecommons.org/licenses/by/4.0/>.

© The Author(s) 2024